J|A|C|S
ARTICLES
Published on Web 04/03/2004

Solvent Dependence of Intramolecular Electron Transfer in a Helical Oligoproline Assembly

Durwin R. Striplin,*,† Steven Y. Reece,† Dewey G. McCafferty,‡,|| Craig G. Wall,‡ Duane A. Friesen,‡ Bruce W. Erickson,‡,⊥ and Thomas J. Meyer*,§

Contribution from the Department of Chemistry, Davidson College, Davidson, North Carolina 28036, Department of Chemistry, University of North Carolina at Chapel Hill, Chapel Hill, North Carolina 27514, and Associate Director for Strategic Research, Los Alamos National Laboratory, MS A127, Los Alamos, New Mexico 87545

Received July 14, 2003; E-mail: tjmeyer@lanl.gov

Abstract: The helical oligoproline assembly CH_3-CO-Pro-Pro-Pro-Pra(Ptzpn)-Pro-Pro-Pra($Ru^{II}b_2m$)$^{2+}$-Pro-Pro-Pra(Anq)-Pro-Pro-Pro-NH_2, having a spatially ordered array of functional sites protruding from the proline backbone, has been prepared. The 13-residue assembly formed a linear array containing a phenothiazine electron donor, a tris(bipyridine)ruthenium(II) chromophore, and an anthraquinone electron acceptor with the proline II secondary structure as shown by circular dichroism measurements. Following $Ru^{II} \rightarrow b_2m$ metal-to-ligand charge-transfer (MLCT) excitation at 457 nm, electron-transfer quenching occurs, ultimately to give a redox-separated (RS) state containing a phenothiazine (PTZ) radical cation at the Pra(Ptzpn) site and an anthraquinone (ANQ) radical anion at the Pra(Anq) site. The redox-separated state was formed with 33−96% efficiency depending on the solvent, and the transient stored energy varied from −1.46 to −1.71 eV at 22 ± 2 °C. The dominant quenching mechanism is PTZ reductive quenching of the initial $Ru^{III}(b_2m^{\bullet-})$ MLCT excited state which is followed by $m^{\bullet-} \rightarrow$ ANQ electron transfer to give the RS state. Back electron transfer is highly exergonic and occurs in the inverted region. The rate constant for back electron transfer is solvent dependent and varies from 5.2×10^6 to 7.7×10^6 s^{-1} at 22 ± 2 °C. It is concluded that back electron transfer occurs by direct $ANQ^{\bullet-} \rightarrow PTZ^{\bullet+}$ electron transfer. Based on independently evaluated kinetic parameters, the electron-transfer matrix element is $H_{DA} \approx 0.13$ cm^{-1}.

Introduction

The biological photosynthetic reaction center contains a spatially ordered array of chromophores and electron-transfer donors and acceptors that efficiently separate reductive and oxidative equivalents upon irradiation with visible light. Artificial systems have been prepared which mimic the excitation redox separation characteristics of the reaction center of photosynthesis.[1−11] One long-range goal of these studies is the construction of light-harvesting arrays that can be used as molecular-photochemical or photochemical-electrochemical reactors.[12]

In an earlier, preliminary account, we described a spatially ordered electron-transfer donor/chromophore/acceptor array based on a 13-residue proline II helix, **1**.[13a] This oligoproline assembly which bears three different redox sites is pictured in Figure 1. Circular dichroism studies show that this array adopts the left-handed proline II helix in both water and acetonitrile.[13] The proline II helix repeats itself every three residues with a repeat spacing of 9.4 Å. The right-handed proline I helix is normally favored in relatively nonpolar solvents such as acetonitrile. However, its repeat spacing is 6.3 Å. The relatively large volumes of the donor/chromophore/acceptor groups appear

† Davidson College.
‡ University of North Carolina at Chapel Hill.
§ Los Alamos National Laboratory.
|| Present address: Department of Biochemistry and Biophysics, University of Pennsylvania Health System, Philadelphia, PA.
⊥ Deceased.

(1) Balzani, V. *Supramolecular Photochemistry*; Balzani, V., Ed.; D. Reidel: Amsterdam, 1989.
(2) Gust, D.; Moore, T. A. *Science* **1989**, *244*, 35.
(3) Gust, D.; Moore, T. A. *Adv. Photochem.* **1991**, *16*, 1.
(4) Meyer, T. J. *Acc. Chem. Res.* **1989**, *22*, 163.
(5) Wasielewski, M. R. Electron Transfer Reactions in Metalloproteins. In *Metal Ions in Biological Systems*; Sigel, H., Sigel, A., Eds.; Marcel Dekker: New York, 1991; Vol. 27, p 361.
(6) Wasielewski, M. R. *Chem. Rev.* **1992**, *92*, 435.
(7) Bolton, J. R.; Mataga, N.; McLendon, G. In *Electron Transfer in Inorganic, Organic, and Biological Systems*; Bolton, J. R., Mataga, N., McLendon, G., Eds.; American Chemical Society and Canadian Society for Chemistry: Washington, DC and Ottawa, 1991; Vol. 228.
(8) *Photoinduced Electron Transfer*; Fox, M. A., Chanon, M., Eds.; Elsevier: Amsterdam, 1988; Vols. A−D.
(9) Photoinduced Electron-Transfer I−V. *Topics in Current Chemistry*; Mattay, J., Ed.; Springer-Verlag: Berlin, 1990−1993; Vols. 156, 158, 159, 163, 168.
(10) Ogawa, M. Y. Electron Transfer Within Synthetic Polypeptides and De Novo Designed Proteins. In *Molecular and Supramolecular Photochemistry: Multimetallic and Macromolecular Inorganic Photochemistry*; Ramamurthy, V., Schanze, K. S., Eds.; Marcel Dekker: New York, 1999; Vol. 4, pp 113−150.
(11) Schanze, K. S.; Walters, K. A. Photoinduced Electron Transfer in Metal-Organic Dyads. In *Molecular and Supramolecular Photochemistry: Organic and Inorganic Photochemistry*; Ramamurthy, V., Schanze, K. S., Eds.; Marcel Dekker: New York, 1998; Vol. 2, pp 75−127.
(12) *Photochemical Processes in Organized Molecular Systems*; Meyer, T. J., Honda, K., Eds.; Elsevier: Yokohama, Japan, 1991; p 133.
(13) (a) McCafferty, D. G.; Friesen, D. A.; Danielson, E.; Wall, C. G.; Saderholm, M. J.; Erickson, B. W.; Meyer, T. J. *Proc. Natl. Acad. Sci. U.S.A.* **1996**, *93*, 8200. (b) Slate, C.; Binstead, R.; Meyer, T.; Erickson, B. *Lett. Pet. Sci.* **1999**, *6*, 61−69.

10.1021/ja0304289 CCC: $27.50

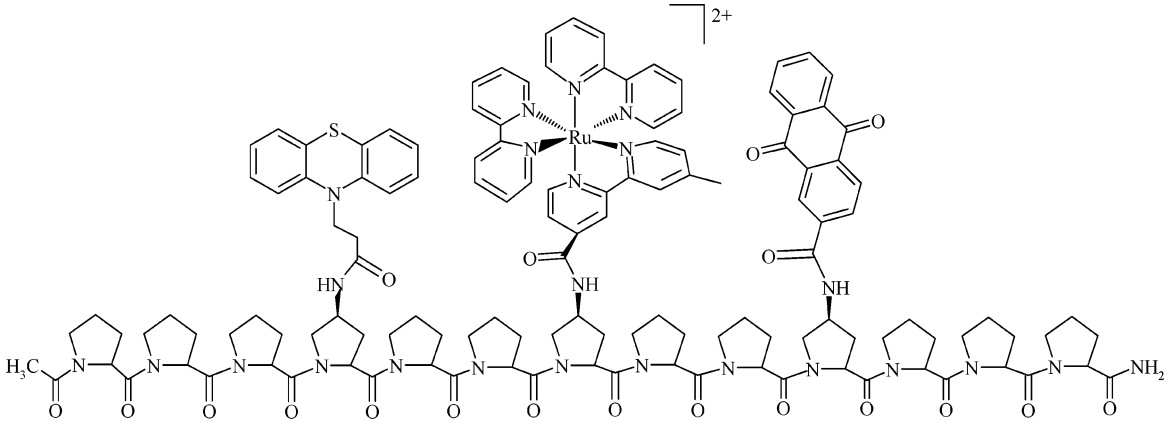

CH_3-CO-Pro-Pro-Pro-Pra(Ptzpn)-Pro-Pro-Pra($Ru^{II}b_2m$)$^{2+}$-Pro-Pro-Pra(Anq)-Pro-Pro-Pro-NH_2

1

Figure 1. Covalent structure of oligoproline assembly **1**.

Scheme 1

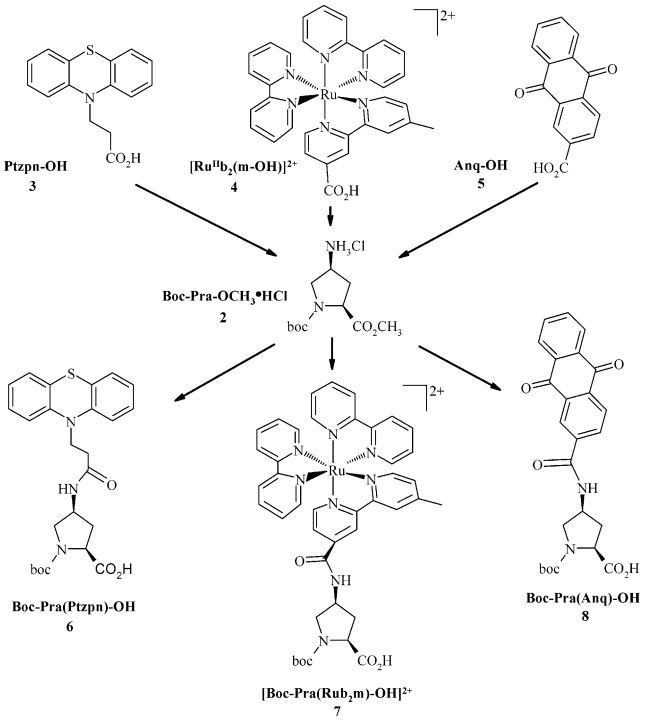

to favor the more open proline II structure even in nonpolar solvents to decrease steric repulsion.

The synthetic strategy adopted for preparing the redox modules that were incorporated into the final assembly is shown in Scheme 1. The oligoproline system was subsequently assembled by manual solid-phase synthesis on methylbenzhydrylamine-resin from N^{α}-(1,1-dimethylethoxycarbonyl)-proline (Boc-Pro-OH), N^{α}-(1,1-dimethylethoxycarbonyl)-L-prolyl-L-proline-OH (Boc-Pro-Pro-OH), and redox modules **6**−**8** shown in Scheme 1. The three redox-active modules were synthesized from their corresponding acids, **3**−**5**, by coupling them to the 4-amino group of Boc-amino ester, **2**. Subsequent saponification of the methyl ester with lithium hydroxide provided a redox Boc-amino acid for use in the solid-phase peptide synthesis.[14]

(14) Erickson, B. W.; Merrifield, R. B. *Proteins* **1976**, *2*, 255.

Scheme 2

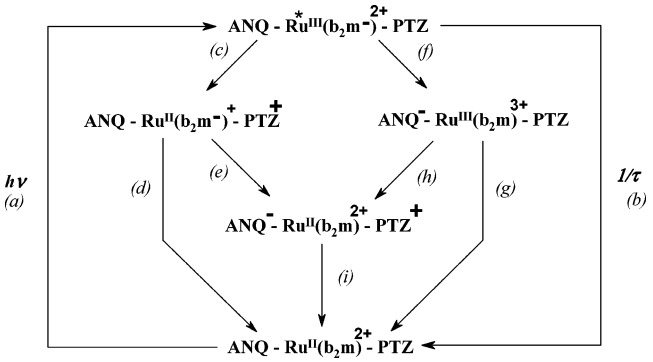

Scheme 2 outlines the kinetic pathways that can occur following irradiation of assembly **1** with visible light. The ruthenium polypyridyl complex is the visible light absorber (reaction *a*). Absorption of light produces a metal-to-ligand charge-transfer, MLCT, excited state. The metal complex is unsymmetrical with the lowest MLCT state based on 4′-methyl-2,2′-bipyridine-4-carbonyl as the acceptor ligand as shown by transient resonance Raman measurements.[15]

Once formed, the excited state can return to the ground state directly by a combination of radiative and nonradiative pathways, (*b*) in Scheme 2, or be quenched by donating an electron from the reduced ligand to the anthraquinone electron acceptor (*f*) or by accepting an electron from phenothiazine (*c*). Subsequent electron transfer from PTZ to Ru^{III} in (*h*) or from reduced ligand m^- to the quinone in (*e*) leads to the lowest state energetically, the redox-separated (RS) state. It contains oxidized phenothiazine (PTZ^+) and reduced anthraquinone (ANQ^-) separated by a five-proline array spacer. The RS state returns to the ground state by back electron transfer in (*i*). Back electron transfer could occur by any or a combination of three pathways including: (1) long-range through-space and/or through-bond $ANQ^- \rightarrow PTZ^+$ electron transfer, (2) $ANQ^- \rightarrow m$ electron transfer followed by $m^- \rightarrow PTZ^+$ back electron transfer, note Scheme 2, and (3) $Ru^{II} \rightarrow PTZ^+$ electron transfer followed by $ANQ^- \rightarrow Ru^{III}$ electron transfer.

(15) Dupray, L. M.; Devenney, M.; Striplin, D. R.; Meyer, T. J. *J. Am. Chem. Soc.* **1997**, *119*, 10243−10244.

We describe here the details of the construction of helical oligoproline assembly **1** and its photophysical and electrochemical properties including the influence of solvent on emission energies, lifetimes, quantum yields, and electron-transfer dynamics. An analysis of these data provide insight into the mechanisms of both electron-transfer quenching and back electron transfer which occurs in the inverted region. One limitation in this study was the inability to use water as a solvent because of its deleterious effect on the ANQ radical anion once formed.

Experimental Section

Materials. The following compounds were prepared according to literature procedures: *cis*-1-(1,1-dimethylethoxycarbonyl)-4-amino-L-proline methyl ester hydrochloride, Boc-Pra-OCH_3·HCl (**2**);[16] 3-(10*H*-phenothiazine-10)propanoic acid, Ptzpn-OH (**3**);[17] bis(2,2′-bipyridine)-(4′-methyl-2,2′-bipyridine-4-carboxylic acid) ruthenium(II)bis(hexafluorophosphate), $[Ru^{II}b_2(m\text{-}OH)](PF_6)_2$ (**4**).[17] The following compounds and materials were purchased: anthraquinone-2-carboxylic acid, Anq-OH (**5**) (Aldrich); N^{α}-(1,1-dimethylethoxycarbonyl)-L-prolyl-L-proline-OH, Boc-Pro-Pro-OH (Fluka); N^{α}-(1,1-dimethylethoxycarbonyl)-proline, Boc-Pro-OH (Aldrich); methylbenzhydrylamine-*copoly*-(styrene-1% divinylbenzene) beads (MBHA resin, Applied Biosystems, 0.62 mmol/g substitution). Acetonitrile, ACN (Burdick and Jackson), butyronitrile, BuCN (Aldrich gold-label 99.9%), *N*,*N*-dimethylacetamide, DMA (Aldrich gold-label 99.9%), and 1,2-dichloroethane, DCE (Fisher AR grade), were dried and purified by stirring with 4 Å molecular sieve dust under argon for 1 h followed by filtration through a 5 cm × 15 cm column of activity-grade I neutral alumina and were stored under argon. This treatment removed reducing impurities and water from the solvents, which was required to avoid photochemically induced degradation of the anthraquinone group.

General Methods. Melting points were measured on a Thomas-Hoover apparatus and are uncorrected. UV−vis spectra were recorded on a Hewlett-Packard model 8452A spectrophotometer. ^{1}H NMR spectra were recorded on Varian 400-MHz, Bruker 250-MHz, or Bruker 200-MHz spectrometers. Chemical shifts are reported in parts per million downfield from internal $(CH_3)_4Si$ (δ). Flash chromatography was performed with a silica gel (Baker, 60−200 mesh) or neutral alumina (Fisher, 80−200 mesh) column. Thin-layer chromatography was carried out with silica gel (Whatman Diamondback) or alumina (Bakerflex) analytical plates. Atlantic Microlab (Norcross, GA) performed elemental analyses. Positive-ion fast bombardment mass spectra (FAB-MS) were recorded with a VG SEQ70 hybrid MS/MS spectrometer. Samples were immobilized in either a dithiothreitol-dithioerythritol matrix ("magic bullet") or a nitrobenzyl alcohol matrix (for organometallics).

***cis*-N^{α}-(1,1-Dimethylethoxycarbonyl)-4-(3-(10*H*-phenothiazine-10)propanoyl)-4-amino-L-proline Methyl Ester, Boc-Pra(Ptzpn)-OCH_3.** Light was excluded from this reaction at all times. Boc-Pra-OCH_3·HCl (**2**) (4.0 mmol, 1.0 equiv), PTZpn-OH (**3**) (4.0 mmol, 1.0 equiv), and *N*-methylmorpholine (NMM, 12.3 mmol, 3.3 equiv) were dissolved in a minimum amount of dichloromethane with stirring. Solid dicyclohexylcarbodiimide (DCC, 4.1 mmol, 1.1 equiv) and 4-(dimethylamino)pyridine (0.4 mmol, DMAP, 0.1 equiv) were added, and the solution was stirred at room temperature for 16 h. One drop of acetic acid was added, and the mixture was stirred for an additional 30 min. The precipitated dicyclohexylurea (DCU) was filtered and washed with CH_2Cl_2. The filtrate was dried with Na_2SO_4 and evaporated to dryness by rotary evaporation. The residual oil was solidified by trituration with hexanes and collected by filtration. The pinkish-white solid was chromatographed on silica gel with 1:1 ethyl acetate/hexanes (v/v). Fractions containing the desired product were dried with anhydrous Na_2SO_4 and freed of solvent by rotary evaporation to provide the title compound, Boc-Pra(Ptzpn)-OCH_3, as a pinkish-white solid (1.67 g, 84% yield): mp 76.0−78.0 °C. UV−vis (CH_3CN): λ (ϵ) 232 (16 200), 254 (46 500), and 308 nm (5800 L cm^{-1} mol^{-1}). FAB-MS (calcd for $C_{26}H_{31}N_3O_5S$ [MH^+]: *m*/*z* 497.608): *m*/*z* 497 (MH^+), 441, 398 (MH^+ − Boc), 252, 226, 212, 198, 180. ^{1}H NMR (200 MHz, $CDCl_3$): δ 1.38 (s, 9H, $(CH_3)_3C$), 1.84 (m, 1H, $C^{\beta}H$), 2.40 (m, 1H, $C^{\beta}H$), 2.62 (t, $J_{2',3'} = 6.9$ Hz, 2H, 2′-CH_2), 3.31−3.61 (m, 2H, $C^{\delta}H_2$), 3.66 (2 s, 3H, OCH_3), 4.14−4.25 (m, 1H, $C^{\alpha}H$), 4.20 (t, $J_{2',3'} = 7.0$ Hz, 2H, 3′-CH_2), 4.57 (m, 1H, $C^{\gamma}H$), 6.76 (m, 1H, $N^{\gamma}H$), and 6.88−7.19 (m, 8H, C_8H_8NS). Anal. Calcd for $C_{26}H_{31}N_3O_5S$: C, 62.76; H, 6.73; N, 8.44; S, 6.44. Found: C, 62.84; H, 6.67; N, 8.30; S, 6.38.

***cis*-N^{α}-(1,1-Dimethylethoxycarbonyl)-4-(3-(10*H*-phenothiazine-10)propanoyl)-4-amino-L-proline, Boc-Pra(Ptzpn)-OH (6).** Light was excluded from this reaction at all times. A suspension of Boc-Pra-(Ptzpn)-OCH_3 (1.49 g, 3.0 mmol, 1.0 equiv) in 3:1 methanol/water (v/v) (35 mL) was cooled to 0 °C with stirring. Solid lithium hydroxide (5.0 equiv) was added, and the mixture was stirred without cooling for 16 h, during which it warmed to room temperature. After the methanol was removed by rotary evaporation, the alkaline solution was extracted with CH_2Cl_2 (5 × 25 mL) and acidified to pH 2−3 with 0.1 M HCl. The light purple gum that precipitated was partitioned between ethyl acetate and water and extracted into ethyl acetate (5 × 30 mL). The organic phase was dried over anhydrous $MgSO_4$ and freed of solvent to provide pure free acid, Boc-Pra(Ptzpn)-OH, as a light purple solid (1.39 g, 97% yield): mp 115 °C dec. UV−vis (CH_3CN): λ (ϵ) 232 (16 200), 254 (46 500), and 308 nm (5800 L cm^{-1} mol^{-1}). FAB-MS (calcd for $C_{25}H_{29}N_3O_5S$ [MH^+]: *m*/*z* 483.5812): *m*/*z* 483 (MH^+), 438, 428, 406, 383 (MH^+ − Boc), 212, 198, 180. ^{1}H NMR (200 MHz, $CDCl_3$): δ 1.37 (s, 9H, $(CH_3)_3C$), 1.82 (m, 1H, $C^{\beta}H$), 2.41 (m, 1H, $C^{\beta}H$), 2.63 (t, $J_{2',3'} = 6.9$ Hz, 2H, 2′-CH_2), 3.31−3.59 (m, 2H, $C^{\delta}H_2$), 4.20 (t, $J_{2',3'} = 7.0$ Hz, 2H, 3′-CH_2), 4.18−4.22 (m, 1H, $C^{\alpha}H$), 4.56 (m, 1H, $C^{\gamma}H$), and 6.88−7.20 (m, 9H, C_8H_8NS and $N^{\gamma}H$). Anal. Calcd for $C_{25}H_{29}N_3O_5S$: C, 62.09; H, 6.04; N, 8.69; S, 6.63. Found: C, 61.18; H, 6.16; N, 8.60; S, 6.58.

***cis*-N^{α}-(1,1-Dimethylethoxycarbonyl)-4-(bis(2,2′-bipyridine)(4′-methyl-2,2′-bipyridine-4-carboxamide)ruthenium(II)-L-proline Methyl Ester Bis(hexafluorophosphate), $[Boc\text{-}Pra(Rub_2m)\text{-}OCH_3](PF_6)_2$.** Boc-Pra-$OCH_3$·HCl (**2**) (4.0 mmol, 1.0 equiv), $[Ru^{II}b_2(m\text{-}OH)](PF_6)_2$ (**4**) (4.0 mmol, 1.0 equiv), and *N*-methylmorpholine (NMM, 12.3 mmol, 3.3 equiv) were dissolved in a minimum amount of dichloromethane with stirring. Solid dicyclohexylcarbodiimide (DCC, 4.1 mmol, 1.1 equiv) and 4-(dimethylamino)pyridine (DMAP, 0.4 mmol, 0.1 equiv) were added, and the solution was stirred at room temperature for 16 h. One drop of acetic acid was added, and the mixture was stirred for an additional 30 min. The precipitated dicyclohexylurea (DCU) was filtered and washed with CH_2Cl_2. The filtrate was dried with Na_2SO_4 and evaporated to dryness by rotary evaporation. The residual blood-red oil was chromatographed on neutral alumina by using 2:1 acetonitrile/toluene (v/v). The fractions containing the desired product were freed of solvent by rotary evaporation. The remaining oil was redissolved in acetonitrile (1 mL) and dripped into rapidly stirring ice-cold diethyl ether (200 mL). The bright orange solid that precipitated was collected on a medium porosity glass frit and vacuum-dried to afford pure $[Boc\text{-}Pra(Rub_2m)\text{-}OCH_3](PF_6)_2$ (3.76 g, 82% yield): mp 204 °C dec. UV−vis (CH_3CN): λ (ϵ) 246 (21 700), 288 (54 300), and 456 nm (11 700 L cm^{-1}mol^{-1}). FAB-MS (calcd for $C_{43}H_{44}N_8O_5RuP_2F_{12}$ [$(M - PF_6)^+$]: *m*/*z* 998.9054, [$(M - 2PF_6)^+$]: *m*/*z* 853.9412): *m*/*z* 999 $(M - PF_6)^+$, 854 $(M - 2PF_6)^+$, 761, 452, 396. ^{1}H NMR (200 MHz, CD_3CN): δ 1.37 (2 s, 9H, $(CH_3)_3C$), 1.87−1.92 (m, 2H, $C^{\beta}H$), 2.52−2.58 (m, 1H, $C^{\beta}H$), 2.54 (s, 2H, m-CH_3), 3.35−3.74 (m, 2H, $C^{\delta}H_2$), 3.71 (s, 3H,

(16) McCafferty, D. G.; Slate, C. A.; Nakhle, B. M.; Graham, H. D. J.; Austell, T. L.; Vachet, R. W.; Mullis, B. H.; Erickson, B. W. *Tetrahedron* **1995**, *51*, 9859.
(17) McCafferty, D. G.; Bishop, B. M.; Wall, C. G.; Hughes, S. G.; Mecklenburg, S. L.; Meyer, T. J.; Erickson, B. W. *Tetrahedron* **1995**, *51*, 1093.

OCH_3), 4.30 (d, J = 9.4 Hz, d, J = 4.3 Hz, 1H, $C^{\alpha}H$), 4.64 (m, 1H, $C^{\gamma}H$), 7.27 (m, 1H, m5′), 7.30−7.37 (m, 4H, 4 × b5), 7.51−7.92 (m, 8H, 4 × b6 and m5 and m6′ and m6 and $N^{\alpha}H$), 8.00−8.08 (m, 5H, 4 × b4 and $N^{\epsilon}H$), 8.45−8.50 (m, 5H, 4 × b3 and m3′), and 8.75 ppm (br s, 1 H, m3). Anal. Calcd for $C_{43}H_{44}N_8O_5RuP_2F_{12}$: C, 45.15; H, 3.88; N, 9.80. Found: C, 45.27; H, 4.09; N, 9.71.

***cis*-N^{α}-(1,1-Dimethylethoxycarbonyl)-4-(bis(2,2′-bipyridine)(4′-methyl-2,2′-bipyridine-4-carboxamide)ruthenium(II)-L-proline Bis-(hexafluorophosphate), [Boc-Pra(Rub_2m)-OH]$(PF_6)_2$ (7).** A suspension of [Boc-Pra(Rub_2m)-OCH_3]$(PF_6)_2$ (1.76 g, 1.5 mmol, 1.0 equiv) in 3:1 methanol/water (v/v) (25 mL) was cooled to 0 °C with stirring. Solid lithium hydroxide (5.0 equiv) was added, and the mixture was stirred without cooling for 16 h, during which it warmed to room temperature. After the methanol was removed by rotary evaporation, the alkaline solution was acidified with 0.1 M HPF_6 and extracted with CH_2Cl_2 (5 × 25 mL). The organic phase was dried over anhydrous $MgSO_4$ and freed of solvent to provide the free acid as a red oil. The oil was dissolved in acetonitrile (1 mL) and dripped into rapidly stirring ice-cold diethyl ether (200 mL). The bright red-orange solid that precipitated was collected on a medium-porosity glass frit and vacuum-dried to afford pure [Boc-Pra(Rub_2m)-OH]$(PF_6)_2$ (1.68 g, 99% yield): mp 237 °C dec. UV−vis (CH_3CN): λ (ϵ) 246 (21 500), 288 (54 300), and 456 nm (11 700 L cm^{-1} mol^{-1}). FAB-MS (calcd for $C_{42}H_{42}N_8O_5RuP_2F_{12}$ [$(M - PF_6)^+$]: m/z 984.8786, [$(M - 2PF_6)^+$]: m/z 839.9144): m/z 985 $(M - PF_6)^+$, 839 $(M - 2PF_6)^+$, 794, 773, 695, 659, 615, 569. ^{1}H NMR (200 MHz, CD_3CN): δ 1.37 (2 s, 9H, $(CH_3)_3C$), 1.87−1.90 (m, 2H, $C^{\beta}H$), 2.52−2.58 (m, 1H, $C^{\beta}H$), 2.54 (s, 2H, m-CH_3), 3.36−3.78 (m, 2H, $C^{\delta}H_2$), 4.33 (m, 1H, $C^{\alpha}H$), 4.58 (m, 1H, $C^{\gamma}H$), 7.25 (d, $J_{5',6'}$ = 5.9 Hz, 1H, m5′), 7.34−7.39 (m, 4H, 4 × b5), 7.53 (d, $J_{5,6}$ = 5.8 Hz, 1H, m5), 7.60−7.70 (m, 6H, 4 × b6 and m6′ and $N^{\alpha}H$), 7.84 (d, $J_{5,6}$ = 5.8 Hz, 1H, m6), 7.80−8.08 (m, 5H, 4 × b4 and $N^{\gamma}H$), 8.47 (2 br s, 5H, 4 × b3 and m3′), and 8.75 ppm (br s, 1H, m3). Anal. Calcd for $C_{42}H_{42}N_8O_5RuP_2F_{12}$: C, 44.65; H, 3.75; N, 9.92. Found: C, 44.58; H, 3.84; N, 9.85.

***cis*-N^{α}-(1,1-Dimethylethoxycarbonyl)-4-(9,10-dihydro-9,10-dioxoanthracene-2-carboxamide)-L-proline Methyl Ester, Boc-Pra(Anq)-OCH_3.** Boc-Pra-OCH_3·HCl (**2**) (4.0 mmol, 1.0 equiv), Anq-OH (**5**) (4.0 mmol, 1.0 equiv), and *N*-methylmorpholine (NMM, 12.3 mmol, 3.3 equiv) were suspended in *N*,*N*-dimethylformamide (DMF, 20 mL) with stirring. Solid dicyclohexylcarbodiimide (DCC, 4.1 mmol, 1.1 equiv) and 4-(dimethylamino)pyridine (0.4 mmol, DMAP, 0.1 equiv) were added, and the creamy solution was stirred at room temperature for 16 h. One drop of acetic acid was added, and the mixture was stirred for an additional 30 min. The precipitated dicyclohexylurea (DCU) was filtered and washed with DMF. The filtrate was evaporated to a yellow solid by rotary evaporation under reduced pressure (0.2 Torr). The solid was chromatographed on silica gel by using 1:1 hexanes/ethyl acetate as the eluent. The organics were dried over anhydrous $MgSO_4$ and freed of solvent to afford the title compound, Boc-Pra(Anq)-OCH_3, as a yellow solid (0.386 g, 21% yield): mp 256 °C dec. UV−vis (CH_3CN): λ (ϵ) 210 (41 100), 256 (60 500), and 326 nm (7500 L cm^{-1} mol^{-1}). FAB-MS (calcd for $C_{26}H_{26}N_2O_7$ [MH^+]: m/z 478.5006): m/z 479 (MH^+), 379 (MH^+ − Boc), 334, 252, 235, 225, 208. ^{1}H NMR (250 MHz, $CDCl_3$): δ 1.45 (2 s, 9H, $(CH_3)_3C$), 2.02 (m, 1H, $C^{\beta}H$), 2.56 (m, 1H, $C^{\beta}H$), 3.73 (m, 2H, $C^{\delta}H_2$), 3.85 (s, 3H, OCH_3), 4.33−4.43 (2 d, J = 8.4 Hz, 1H, $C^{\alpha}H$), 4.93 (m, 1H, $C^{\gamma}H$), 7.79−7.83 (m, 2H, 6,7-Anq), 8.29−8.33 (m, 5H, 3,4,5,8-Anq and $N^{\gamma}H$), and 8.63 ppm (2 s, 1H, 1-Anq). Anal. Calcd for $C_{26}H_{26}N_2O_7$: C, 65.26; H, 5.48; N, 5.85. Found: C, 65.46; H, 5.56; N, 5.71.

***cis*-N^{α}-(1,1-Dimethylethoxycarbonyl)-4-(9,10-dihydro-9,10-dioxoanthracene-2-carboxamide)-L-proline, Boc-Pra(Anq)-OH (8).** A suspension of Boc-Pra(Anq)-OCH_3 (0.386 g, 0.81 mmol, 1.0 equiv) in 3:1 methanol/water (v/v) (15 mL) was cooled to 0 °C with stirring. Solid lithium hydroxide (5.0 equiv) was added, and the mixture was stirred without cooling for 16 h, during which it warmed to room temperature. After the methanol was removed by rotary evaporation, the alkaline solution was extracted with CH_2Cl_2 (5 × 25 mL) and acidified to pH 2−3 with 0.1 M HCl. The resulting yellow precipitant was collected by filtration, washed with water, and dried in a vacuum desiccator overnight. The acid product, Boc-Pra(Anq)-OH (0.365 g, 97% yield), was judged to be homogeneous by TLC (silica gel, 1:1 ethyl acetate/hexanes) and ^{1}H NMR: mp 256 °C dec. UV−vis (CH_3CN): λ (ϵ) 256 (33 900), and 326 nm (4800 L cm^{-1} mol^{-1}). FAB-MS (calcd for $C_{25}H_{24}N_2O_7$ [MH^+]: m/z 464.4738): m/z 465 (MH^+), 409, 365 (MH^+ − Boc), 309, 235, 155. ^{1}H NMR (250 MHz, 10% $(CD_3)_2CO$ in $CDCl_3$): δ 1.36 (s, 9H, $(CH_3)_3C$), 2.07−2.13 (2 s, 1H, $C^{\beta}H$), 2.49 (m, 1H, $C^{\beta}H$), 3.48−3.62 (m, 2H, $C^{\delta}H$), 4.21−4.25 (2 d, J = 7.7 Hz, 1H, $C^{\alpha}H$), 4.79 (m, 1H, $C^{\gamma}H$), 7.71−7.77 (m, 2H, 6,7-Anq), 8.16−8.37 (m, 4H, 3,4,5,8-Anq), 8.36 (d, J = 8.4 Hz, 1H, $N^{\gamma}H$), and 8.52 ppm (s, 1H, 1-Anq). Anal. Calcd for $C_{25}H_{24}N_2O_7$: C, 64.63; H, 5.21; N, 6.03. Found: C, 65.46; H, 5.99; N, 5.61.

[CH_3-CO-Pro-Pro-Pro-Pra(Ptzpn)-Pro-Pro-Pra($Ru^{II}b_2$m)-Pro-Pro-Pra(Anq)-Pro-Pro-Pro-NH_2]$(PF_6)_2$ (1). This 13-residue peptide amide was assembled by manual solid-phase synthesis by using Boc-Pro-OH, Boc-Pro-Pro-OH, redox modules **6**−**8**, and MBHA resin. The synthetic cycle of Fournier and co-workers[18] was used except that NMM was used for neutralization and the Boc-amino acid (4.0 equiv), BOP (2.2 equiv), HOBt (2.2 equiv), and NMM (4.2 equiv) were used for coupling. Boc-Pra($Ru^{II}b_2$m)-OH (2.0 equiv) was coupled for 18 h.[19] Prior to cleavage, the resin-bound peptide was N-terminally acetylated with acetic anhydride (Ac_2O) in CH_2Cl_2. The peptide was cleaved from the resin with 10:1 (v/v) HF/anisole (1 h, 4 °C) in the presence of 2-mercaptopyridine (1 mmol) to prevent oxidation of phenothiazine to the sulfoxide. The crude peptide was purified by preparative reversed-phase HPLC on a butyl-silica column (Vydac C_4) eluted over 90 min with a linear gradient of 25−39% acetonitrile in 0.5% trifluoroacetic acid/water. The center fractions were freed of solvent to provide pure peptide as an orange powder (66 mg). EI-MS calcd. for $C_{129}H_{140}N_{24}O_{19}$-Sru 2462.95 Da, found 2464.2 Da. UV−vis (CH_3CN): λ (ϵ) 254 (77 600), 288 (59 600), 326 sh (11 800), and 456 nm (11 700 L cm^{-1} mol^{-1}).

Electrochemistry. Tetra(1-butyl)ammonium hexafluorophosphate, Bu_4NPF_6 (Aldrich), was twice recrystallized from ethanol and vacuum-dried for 10 h. All halfwave potentials are vs SSCE at a scan rate of 100 mV s^{-1}. Each cyclic voltammogram (CV) was obtained in a 0.1 M Bu_4NPF_6 solution of the given solvent with a computer-interfaced Princeton Applied Research 273 potentiostat/galvanostat, a silver/silver nitrate reference electrode, a platinum-wire coil auxiliary electrode, and a BAS MF-2013 platinum disk working electrode (0.31 cm^2 electrode area).

Excited-State Measurements and Spectral Fitting. All samples were bubble-deoxygenated with high-purity argon for at least 20 min. Emission spectra were collected with a Spex F212 spectrofluorimeter operating in photon-counting mode with a cooled Hamamatsu R666 photomultiplier tube (PMT). Emission was collected at right angles to the 457 nm excitation and corrected for the instrument response by the procedure supplied by the manufacturer. For the purposes of spectral fitting and quantum yield measurements, emission spectra were converted to an abscissa linear in energy as described elsewhere.[20,21] Emission quantum yields, ϕ_{em}, were measured in optically dilute solutions relative to $[Ru^{II}(bpy)_3](PF_6)_2$ in CH_3CN at 295 K (ϕ_{em} = 0.0615).[22] Corrections for differences in refractive indices of the

(18) Fournier, A.; Wang, C. T.; Felix, A. M. *Int. J. Pept. Protein Res.* **1988**, *31*, 86.
(19) Peek, B. M.; Ross, G. T.; Edwards, S. W.; Meyer, G. J.; Meyer, T. J.; Erickson, B. W. *Int. J. Pept. Protein Res.* **1991**, *38*, 114.
(20) Allen, G. H.; White, R. P.; Rillema, D. P.; Meyer, T. J. *J. Am. Chem. Soc.* **1984**, *106*, 2613.
(21) Parker, C. A.; Rees, W. T. *Analyst (London)* **1960**, *85*, 857.
(22) Caspar, J. V.; Meyer, T. J. *J. Am. Chem. Soc.* **1989**, *111*, 7448.

Table 1. Reduction Potentials (V vs SSCE) and Calculated Free Energies (eV) at 22 ± 2 °C[a]

solvent[b]	$Ru^{3+/2+}$ (V)	$PTZ^{+/0}$ (V)	$Anq^{0/-}$ (V)	$b_2m^{0/-}$ (V)	$(PTZ^{\bullet+})(Ru^{II}b_2m^{\bullet-})(ANQ)$ (eV)[c]	$(PTZ)(Ru^{III}b_2m)(ANQ^{\bullet-})$ (eV)[e]	$(PTZ^{\bullet+})(ANQ^{\bullet-})$ (eV)[d]
DCE	+1.42	+0.76	−0.83	−1.15	1.75	2.09	1.51
BuCN	+1.45	+0.79	−0.95	−1.10	1.82	2.33	1.71
ACN	+1.31	+0.73	−0.81	−1.10	1.79	2.08	1.52
DMA		+0.75	−0.73	−1.23	1.94		1.46

[a] Free energies were calculated for 0.1 M Bu_4NPF_6 solutions with eq 7, see text. D_s values were found in the *Handbook of Chemistry and Physics*, 80th ed.; Lide, D. R., Ed.; CRC Press: Boca Raton, FL, 1999. [b] DCE, dichloroethane; BuCN, butyronitrile; ACN, acetonitrile; DMA, dimethylacetamide. [c] d = 9 Å, Figure 2. [d] d = 9 Å, Figure 2. [e] d = 18 Å, Figure 2.

solvent and of absorption band intensities were made by using eq 1.[23]

$$\phi_{cm} = \phi_{ref}\frac{A_r}{A_s}\frac{I_s}{I_r}\left(\frac{n_s}{n_r}\right)^2 \quad (1)$$

In eq 1, I is the integrated intensity of the emission manifold, A is the absorbance at the excitation wavelength, and n is the refractive index of the solvent. The relationship between the quantum yield and radiative, k_r, and nonradiative, k_{nr}, rate constants for excited-state deactivation (assuming that the emitting state is formed with unit efficiency) is given in eq 2.

$$\phi_{cm} = \frac{k_r}{k_r + k_{nr}} = k_r\tau \quad (2)$$

In eq 2, τ is the emission decay lifetime.[24]

Emission spectra were analyzed by a standard Franck−Condon analysis as described elsewhere.[25−27] The spectra were fit to eq 3

$$I(\bar{\nu}) = \sum_{\upsilon}^{5}\left\{\left(\frac{E_o - \upsilon\hbar\omega}{E_o}\right)^3\left(\frac{S^{\upsilon}}{\upsilon!}\right)\exp\left[-4\ln 2\left(\frac{\bar{\nu} - E_o - \upsilon\hbar\omega}{\Delta\bar{\nu}_{1/2}}\right)^2\right]\right\} \quad (3)$$

in which $I(\bar{\nu})$ is the emitted intensity in quanta at energy $\bar{\nu}$ in cm^{-1} relative to that for the 0−0 transition. The quantity E_o is the $\upsilon^* = 0 \rightarrow \upsilon = 0$ energy difference between the excited and ground states in the single-mode approximation. The quantity υ is the vibrational quantum number for the average acceptor mode in the ground state, and $\hbar\omega$ is the vibrational spacing. Calculated emission profiles were generated by using eq 3 and were compared to measured spectra by using WINFIT, a least-squares fitting program based on a simplex algorithm written by J. P. Claude.[28]

For bpy-based MLCT excited states, the acceptor mode is the average of a series of coupled υ(bpy) modes from 1100 to 1650 cm^{-1}.[25,26,29,30] The quantity S is the dimensionless Huang−Rhys factor or electron-vibrational coupling constant. It is proportional to the square of the change in equilibrium displacement for the averaged mode between the excited and ground states. The quantity $\Delta\bar{\nu}_{1/2}$ is the full width at half-maximum. It is related to the sum of the solvent reorganizational energy, λ_o, and the reorganizational energy contributed by low-frequency modes treated classically, $\lambda_{i,L}$, as shown in eq 4

$$\lambda_{o,L} = \lambda_o + \lambda_{i,L} = \frac{(\Delta\bar{\nu}_{1/2})^2}{16k_BT\ln(2)} \quad (4)$$

in which k_B is Boltzmann's constant.[30,31] The free energy of the excited state above the ground state, ΔG°_{ES}, is related to E_o by eq 5.[26]

$$\Delta G^\circ_{ES} = E_o + \lambda_{o,L} \quad (5)$$

Emission lifetimes were measured on the samples used to acquire transient absorption spectra by using a PRA LN1000/LN 102 nitrogen laser/dye laser combination operated at 457 nm for sample excitation. Emission was monitored at 90° to the excitation, passed through a dichromate filter to eliminate stray light below 560 nm, and then into a Macpherson 272 scanning monochromator. Emission was monitored with a Hamamatsu R3896 PMT, and the resulting signal was sent to a LeCroy 7200 transient digitizing oscilloscope interfaced to an IBM-PC computer. The decay data were analyzed by exponential or sum of exponential functions, eq 6, with n = 1−3.

$$I(t) = bl + \sum_{i=1}^{n} M_i\exp(-t/\tau_i) \quad (6)$$

In eq 6, $I(t)$ is the emission intensity at time t, τ_i and M_i are the lifetime and preexponential factors for process i, and bl is a baseline correction which was small with our apparatus. Kinetic decay traces were fit to eq 6 by using the nonlinear Marquardt routine.[32]

Nanosecond transient absorption data were obtained following pulsed, right-angle, 457 nm excitation from a Quanta Ray PDL-2 dye laser (coumarin 460 dye) pumped by the third harmonic (355 nm) of a Q-switched Quanta Ray DCR-2A Nd:YAG laser. The probe beam was a 150 W pulsed Xe arc lamp. A shutter placed between the monitoring lamp and the cell was opened for 5 ms intervals to prevent PMT fatigue and sample photolysis. The monitoring light was focused at the cell, collimated after the cell, and finally focused onto the entrance slit of an APL *f*/3.4 grating monochromator. Transient signals were detected by a five-stage Hamamatsu R446 PMT. Spectra were recorded as plots of $\Delta A = \log(I_o/I_t)$ versus monochromator wavelength where I_o was the transmitted light intensity prior to the laser pulse and I_t was the intensity at delay time t. Kinetic decays were analyzed as for emission by using eq 6. Appropriate Oriel or Corning cutoff filters were used to exclude high-energy probe light and direct irradiation of PTZ. The solutions were approximately 1.5×10^{-5} M and bubbled-deoxygenated with high-purity argon for at least 20 min before measurements were initiated.

Results

Electrochemistry. Reduction potentials for **1** measured by cyclic voltammetry in four solvents are tabulated in Table 1. The assignments of the waves were based on voltammograms

(23) Demas, J. N.; Crosby, G. A. *J. Phys. Chem.* **1971**, *75*, 991.
(24) Demas, J. N. *J. Chem. Educ.* **1983**, *60*, 803.
(25) Caspar, J. V.; Westmoreland, T. D.; Allen, G. H.; Bradley, P. G.; Meyer, T. J.; Woodruff, W. H. *J. Am. Chem. Soc.* **1984**, *106*, 3492.
(26) Kober, E. M.; Caspar, J. V.; Lumpkin, R. S.; Meyer, T. J. *J. Phys. Chem.* **1986**, *90*, 3722.
(27) Claude, J. P. Photophysics of Polypyridyl Complexes of Ru(II), Os(II), and Re(I). Ph.D. Thesis, The University of North Carolina at Chapel Hill, Chapel Hill, NC, 1995; p 189.
(28) Caspar, J. V.; Meyer, T. J. *J. Am. Chem. Soc.* **1983**, *105*, 5583.
(29) Chen, P.; Duesing, R.; Graff, D. K.; Meyer, T. J. *J. Phys. Chem.* **1991**, *95*, 5850.
(30) Worl, L. A.; Duesing, R.; Chen, P.; Ciana, L. D.; Meyer, T. J. *J. Chem. Soc., Dalton Trans.* **1991**, 849.
(31) Chen, P.; Meyer, T. J. *Chem. Rev.* **1998**, *98*, 1439−1477.
(32) Marquardt, D. W. *J. Soc. Ind. Appl. Math.* **1963**, *11*, 431.

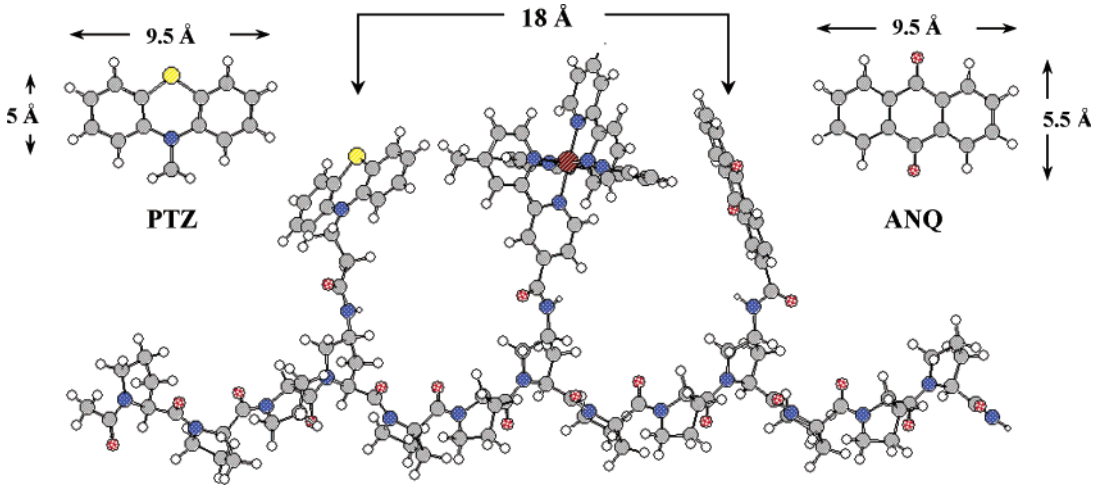

Figure 2. Computer generated structure of the oligoproline assembly. The distance between the ANQ and PTZ modules was measured from the S atom on the PTZ to the center of the ANQ.

Table 2. Solvent-Dependent Emission Data at 22 ± 2 °C[a]

chromophore	solvent[b]	λ_{max}	ϕ_{em} (nm)	M_1	τ_1 (ns)	M_2	τ_2 (ns)	M_3	τ_3 (ns)	*bl*	k_r (10^6 s^{-1})	k_{nr} (10^6 s^{-1})
7	DCE	640	0.102	0.058	1680					0.0009	0.061	0.540
	BuCN	642	0.075	0.065	1360					0.0005	0.055	0.680
	ACN	662	0.090	0.049	1380					0.0003	0.065	0.660
	DMA	648	0.082	0.060	1170					0.0008	0.070	0.780
1	DCE	630	0.033	0.019	38	0.026	390	0.038	1200	−0.0001		
	BuCN	644	0.015	0.048	29	0.017	200	0.024	950	0.0011		
	ACN	653	0.008	0.039	29	0.016	130	0.017	810	−0.0001		
	DMA	652	0.010	0.035	12	0.034	120	0.019	470	0.0006		

[a] Emission decays fit to eq 6. [b] DCE, dichloroethane; BuCN, butyronitrile; ACN, acetonitrile; DMA, dimethylacetamide.

for the individual modules **6**−**8** and earlier results.[13,15,33,34] Differences in potential between isolated modules and peptides were small.

In Table 1, the free energy contents for the various redox states in Scheme 2 above the ground state were calculated by using the electrochemical values. They were calculated from the differences in redox potentials by using eq 7.

$$\Delta G^\circ = \Delta E_{1/2} - \frac{e^2}{D_s d(1+\beta d\mu^{1/2})} \qquad (7)$$

The added term to the redox potential difference is an approximate correction for the Coulombic energy of interaction between the charged redox sites assumed to be spherical ions. The quantities D_s and μ are the dielectric constant and ionic strength of the medium, e is the unit electron charge, d is the separation distance between the ions, and $\beta = (8\pi N_A e^2/1000 D_s k_B T)^{1/2}$.[29,35−41]

The average charge centroid-to-centroid distances were estimated from molecular modeling studies. Low-energy conformations of peptide **1** were explored by molecular mechanics. MM2 energy minimization was performed by using the molecular modeling and analysis program "CS ChemBats3D" (Cambridge Soft Co.: Cambridge, MA). The program employs Allinger's MM2 force field for energy minimization.[42,43] From a variety of starting conformers about the 4-amino substituents, the system equilibrated to a consistent set of low-energy conformers based on the proline II helix. On average, the distance between the S atom on the PTZ to the center of the ANQ was 18 Å, Figure 2. This value is consistent with other modeling studies of analogous oligoproline assemblies.[33,44,45]

Photophysics. The results of steady-state emission and emission decay measurements on chromophore module **7** and peptide triad **1** in four solvents are tabulated in Table 2. Quenching of the chromophore due to its introduction into the peptide was considerable in all cases but solvent dependent. When compared to **7**, emission from **1** was 91% less in acetonitrile, 88% less in dimethylacetamide, 80% less in butyronitrile, and 68% less in dichloroethane.

The results of the application of spectral fitting procedure to the emission bands are summarized in Table 3. It lists the reorganizational energy contributed by solvent and low-frequency modes treated classically, $\lambda_{o,L}$, and the free energies of the excited state above the ground state, ΔG°_{ES}, for **1** and **7**. Reconstruction of the emission bands is very straightforward by using the fitting parameters and eq 3.

(33) Wall, C. W. Directional Electron Transfer at Interfaces. Ph.D. Thesis, The University of North Carolina at Chapel Hill, Chapel Hill, NC, 1995; p 128.
(34) Mecklenburg, S. L.; McCafferty, D. G.; Schoonover, J. R.; Peek, B. M.; Erickson, B. W.; Meyer, T. J. *Inorg. Chem.* **1994**, *33*, 2974−2983.
(35) Meyer, T. J. *Prog. Inorg. Chem.* **1983**, *30*, 389.
(36) Bock, C. R.; Connor, J. A.; Guitierrez, A. R.; Meyer, T. J.; Whitten, D. G.; Sullivan, B. P.; Nagle, J. K. *Chem. Phys. Lett.* **1979**, *61*, 522.
(37) Sutin, N. *J. Photochem.* **1979**, *10*, 19.
(38) Sutin, N. *Acc. Chem. Res.* **1982**, *15*, 275.
(39) Sutin, N. *Prog. Inorg. Chem.* **1983**, *30*, 441.
(40) Newton, M. D.; Sutin, N. *Annu. Rev. Phys. Chem.* **1984**, *35*, 437.
(41) Rehm, D.; Weller, A. *Isr. J. Chem.* **1970**, *8*, 259.
(42) Burkert, U.; Allinger, N. L. *Molecular Mechanics*; American Chemical Society: Washington, DC, 1982.
(43) Clark, T. C. *Computational Chemistry*; Wiley: New York, 1985.
(44) Reece, S. Synthesis and Characterization of Oligoproline Systems Designed for Photoinduced Energy and Electron Transfer. Honors Thesis, Davidson College, Davidson, NC, 2002; p 128.
(45) Serron, S. A.; Aldridge, W. S., III; Fleming, C. N.; Danell, R. M.; Baik, M.; Sykora, M.; Meyer, T. J. *J. Am. Chem. Soc.*, submitted.

Table 3. Emission Spectral Fitting Parameters and Calculated Excited-State Free Energy Values[a]

complex	solvent[b]	E_0 (cm^{-1})	S (cm^{-1})	$\Delta\bar{\nu}_{1/2}$ (cm^{-1})	$\lambda_{o,L}$	ΔG°_{ES} (eV)
7	DCE	16 000	0.85	1890	1570	2.17
	BuCN	16 000	0.93	1880	1550	2.17
	ACN	15 500	0.83	1910	1600	2.11
	DMA	15 700	0.85	1850	1500	2.13
1	DCE	16 400	1.05	1740	1330	2.19
	BuCN	16 000	0.88	1940	1660	2.18
	ACN	15 800	1.02	1830	1470	2.13
	DMA	15 600	0.60	2140	2010	2.18

[a] $\hbar\omega = 1300\ cm^{-1}$. [b] DCE, dichloroethane; BuCN, butyronitrile; ACN, acetonitrile; DMA, dimethylacetamide.

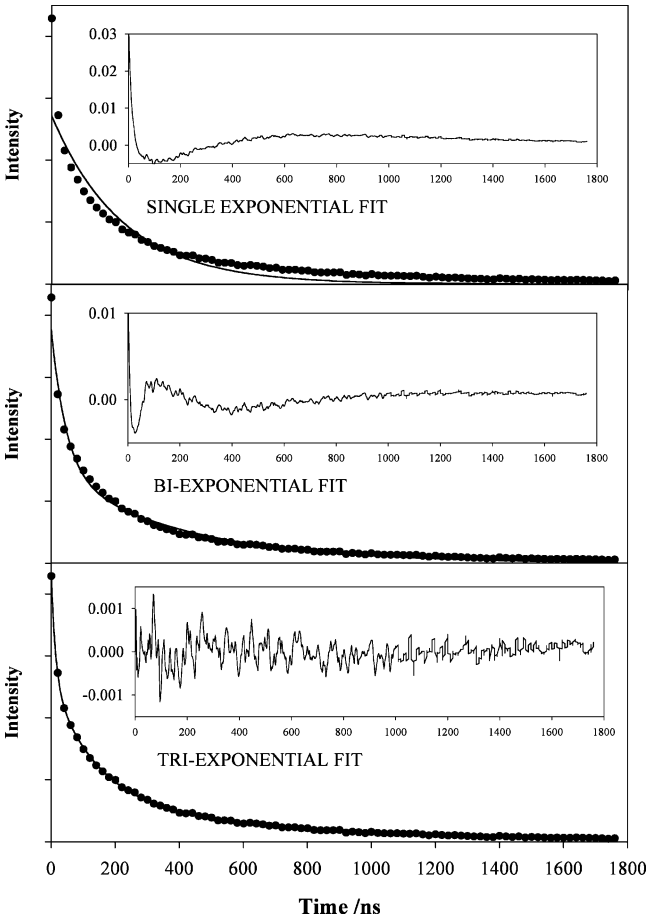

Figure 3. Fitting of an emission decay trace for **1** in dimethylacetamide by using eq 6 varying n from 1 to 3. Inset plots are of the residuals of the calculated fits to the experimental data.

Lifetimes for emission decay for model chromophore **7** in all solvents were single exponential with lifetimes of 1.1 μs and longer ($k \geq 9.1 \times 10^5\ s^{-1}$). The decay kinetics for assembly **1** were complex in all solvents. In Figure 3 is illustrated the effect of varying n from 1 to 3 in eq 6 on the quality of the fits for **1** in dimethylacetamide. The magnitudes and random values of the residuals of the calculated to experimental data were used as the criteria for a successful fit. This comparison illustrates the requirement for use of a triexponential function for fitting the experimental data in all four solvents with the resulting kinetic parameters listed in Table 2.

Transient Absorption Data. A typical transient absorption difference spectrum is shown in Figure 4 as the difference in absorbance before and immediately following laser excitation

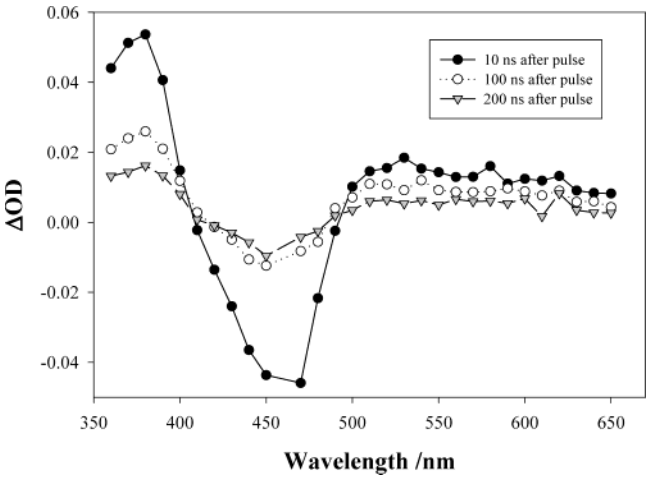

Figure 4. Nanosecond transient absorption difference spectra for **1** in dimethylacetamide at various times following a 4 ns pulse from a 457 nm laser (1.5 mJ/pulse).

Table 4. Solvent Dependence of Kinetic Parameters for Transient Absorption Lifetime Decays for **1** with Fits to Eq 6 as Absorbance Changes with Time, 22 ± 2 °C

monitoring λ (nm)	redox[a] site	M_1	τ_1 (ns)	M_2	τ_2 (ns)	M_3	τ_3 (ns)	*bl*
			Dichloroethane					
370	$b_2m^{\bullet-}$	0.037	22	0.015	130	0.027	750	0.002
450	MLCT	0.140	14	0.020	700			0.002
520	$PTZ^{\bullet+}$	0.019	200					0.001
600	$ANQ^{\bullet-}$	0.015	210					−0.000
			Butyronitrile					
370	$b_2m^{\bullet-}$	0.051	24	0.025	120	0.013	610	0.003
450	MLCT	0.058	17	0.005	1200			−0.002
520	$PTZ^{\bullet+}$	0.038	130					−0.000
600	$ANQ^{\bullet-}$	0.018	130					−0.001
			Acetonitrile					
370	$b_2m^{\bullet-}$	0.043	27	0.019	120	0.012	520	0.009
450	MLCT	0.095	10	0.004	970			−0.001
520	$PTZ^{\bullet+}$	0.041	160					−0.001
600	$ANQ^{\bullet-}$	0.035	160					−0.001
			Dimethylacetamide					
370	$b_2m^{\bullet-}$	0.025	33	0.030	160	0.009	550	−0.000
450	MLCT	0.031	16	0.018	83	0.009	450	0.002
520	$PTZ^{\bullet+}$	0.017	190					0.001
600	$ANQ^{\bullet-}$	0.016	180					0.001

[a] Dominant light absorber.

of **1** in dimethylacetamide. Following the flash, positive absorption features appear at 370 and 520−600 nm. A bleach is also observed near 450 nm. The assignments of these features have been discussed previously.[13] The positive feature at 370 nm is due to the appearance of reduced bipyridine radical, $bpy^{\bullet-}$, and to a small extent reduced anthraquinone, $ANQ^{\bullet-}$. The 450 nm bleach is due to the depletion of the ground-state metal-to-ligand charge-transfer (MLCT) absorption. The 520 feature is due to absorbance by oxidized phenothiazine, PTZ^+, and the absorbance at 580−620 is due to reduced anthraquinone, $ANQ^{\bullet-}$.

The absorption features in Figure 4 are observed for **1** in all four solvents. The lifetimes of the subsequent decays of these features are listed in Table 4. In all four solvents, multiexponential functions with $n = 2$ or 3 in eq 6 were necessary to fit data at 370 and 450 nm, respectively, but decays for PTZ^+ at 520 nm and $ANQ^{\bullet-}$ at 600 nm were single exponential. The

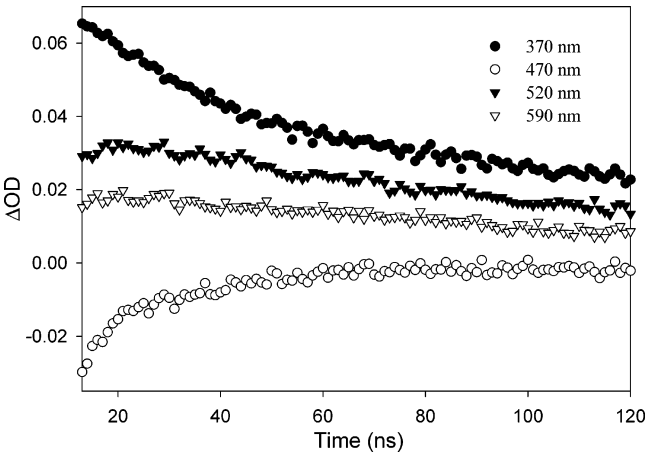

Figure 5. Wavelength dependence of transient absorption changes with time for oligoproline redox triad **1** in butyronitrile, as in Figure 4.

same fitting criterion used for the emission decay fits was used in fitting the transient absorption data.

The decays of the transient absorption features at 370, 470, 520, and 590 nm for **1** in butyronitrile are shown plotted in Figure 5. Typically, the absorbances at 370 and 470 nm reached maximum and minimum values, respectively, before maxima were achieved for the PTZ^+ radical at 520 nm and $ANQ^{\bullet-}$ radical at 590 nm. The kinetics of decay for the absorbance at 370 nm for $bpy^{\bullet-}$ parallel the decay kinetics of the MLCT emission.

Discussion

Electron-Transfer Quenching. The decrease in emission quantum yields as compared to the model complex and the magnitude of the transient absorption spectral changes observed following laser flash photolysis of oligoproline **1** are consistent with considerable electron-transfer quenching. Following MLCT laser flash excitation, electron-transfer quenching occurs in competition with excited-state decay, consistent with Scheme 2.

The kinetic decays for both emission and absorption are complex. Given the circular dichroism evidence, the proline II helical structure is presumably maintained in all solvents.[13] The emission decays are complicated by contributions from a small amount of unquenched emitting impurity most likely due to oxidation of PTZ to the sulfoxide in a fraction of the sample as observed in related samples studied earlier.[17,46,47] Because quenching of the unoxidized sample is efficient, the emitting impurity plays a disproportionate role in the emission decay and yield data, and they must be interpreted with care. The transient absorption data obtained at 370 and 450 nm are complex because of the convolution of absorbance−time changes from residual unquenched excited-state decay, the emitting impurity, and the growth and decay of $PTZ^{\bullet+}$ and $ANQ^{\bullet-}$. Both $PTZ^{\bullet+}$ and $ANQ^{\bullet-}$ appear in all four solvents as shown by the features that appear in the transient absorption spectra at 520 and 600 nm. These are wavelengths where $PTZ^{\bullet+}$ (520 nm) and $ANQ^{\bullet-}$ (600 nm) dominate the absorbance changes. The absorbance decays observed at these wavelengths after the laser flash followed simple exponential kinetics and returned to the baseline for the ground state. The kinetics of decay at either 520 or 600 nm were the same within experimental error, consistent with decay to the ground state by $ANQ^{\bullet-} \rightarrow PTZ^{\bullet+}$ electron transfer. Based on the kinetics data, $k_b = 5.2 \times 10^6$ to 7.7×10^6 s^{-1} depending on the solvent (Tables 4 and 5).

Table 5. Solvent-Dependent Free Energies and Rate Constants for Back Electron Transfer at 22 ± 2 °C

solvent	$\Delta G°$ (eV)	λ_o[a] (eV)	$k_b = k_{ET}$[b] (s^{-1})	calculated H_{DA}[c] (cm^{-1})
DCE	−1.51	0.79	5.2×10^6	0.13
BuCN	−1.71	1.00	7.7×10^6	0.15
ACN	−1.52	1.10	6.3×10^6	0.11
DMA	−1.46	0.51	5.5×10^6	0.11

[a] Calculated from eq 10 with D_s and D_{op} values calculated from data found in the *Handbook of Chemistry and Physics*, 80th ed.; Lide, D. R., Ed.; CRC Press: Boca Raton, FL, 1999, and from Figure 2, $d = 18$ Å and $a_1 = a_2 = 5.0$ Å. [b] Calculated from the average of transient decays between 500 and 620 nm. [c] Calculated from eqs 8 and 9 with $\hbar\omega = 1500$ cm^{-1} and $S = 2.5$.

Because of the response time of the instrument, it was not possible to obtain reliable data for the initial quenching step. A growth in absorbance at both 520 and 600 nm was observed on the 15−20 ns time scale, suggesting that the quenching time scale is 10−20 ns, which suggests $k_q \approx 5 \times 10^7$ to 1×10^8 s^{-1} depending on the solvent with k_q, the rate constant for emission quenching.

Based on the reduction potentials and $\Delta G°$ values in Table 1, initial quenching by reductive PTZ → $Ru^{III}b_2m^{\bullet-}$ electron transfer, reaction (*c*) in Scheme 2, is thermodynamically favored relative to $Ru^{III}b_2m^{\bullet-}$ → ANQ oxidative electron transfer, reaction (*f*). Reductive quenching is favored by $\Delta G°$ values of −0.44, −0.36, −0.34, and −0.24 eV in DCE, BuCN, ACN, and DMA, respectively. In the three solvents where data are available, oxidative quenching by $Ru^{III}b_2m^{\bullet-}$ → ANQ electron transfer is disfavored in BuCN ($\Delta G°$ 0.15 eV) and slightly favored in DCE (−0.10 eV) and ACN (−0.05 eV).

From the simultaneous appearance of $PTZ^{\bullet+}$ and $ANQ^{\bullet-}$, initial PTZ → $Ru^{III}b_2m^{\bullet-}$ quenching is followed by rapid $Ru^{II}b_2m^{\bullet-}$ → ANQ electron transfer. This step is favored by −0.11 to −0.48 eV depending on the solvent, Table 1. The final redox-separated (RS) state is reached by pathway (*c*) followed by (*e*) in Scheme 2.

The quantum yield for maximum formation of the RS state was calculated to be 33%, 54%, 86%, and 43% for **1** in DCE, BuCN, ACN, and DMA, respectively, based on maximum absorbance changes in the absorbance−time traces.[34,47] These values were estimated relative to the efficiency of formation of the MLCT state, $[Ru^{II}(bpy)_3]^*$, in acetonitrile, and are averages of values from maximum ΔOD changes obtained at both 520 and 590 nm. There is a 10−20% error in these values due to the uncertainty in extinction coefficients for $PTZ^{\bullet+}$ and $ANQ^{\bullet-}$ in the different solvents and the extensive overlap of their absorption bands.

The formation yields give additional insight into the steps that dominate electron transfer in Scheme 2. The time scale for quenching (reaction (*c*)) (10−20 ns) is far shorter than the 1170−1680 ns time scale for excited-state decay (reacton (*b*)) of the model MLCT excited state. This is consistent with

(46) Mecklenburg, S. L.; Peek, B. M.; Schoonover, J. R.; McCafferty, D. G.; Wall, C. G.; Erickson, B. W.; Meyer, T. J. *J. Am. Chem. Soc.* **1993**, *115*, 5479−5495.
(47) Chen, P.; Westmoreland, T. D.; Danielson, E.; Schanze, K. S.; Anthon, D.; Neveux, J., P. E.; Meyer, T. J. *Inorg. Chem.* **1987**, *26*, 1116−1126.

assigning much of the residual emission documented in Table 2 to a sulfoxide containing emitting impurity.

With this in mind, quenching yields calculated from $1 - \Phi_{em}(\mathbf{1})/\Phi_{em}$(model), 0.67 (DCE), 0.80 (BuCN), 0.91 (ACN), and 0.88 (DMA), are lower limits. They are still larger than the formation yields by factors as large as 2. Based on these observations, there appears to be a solvent-dependent competition following PTZ $\rightarrow Ru^{III}b_2m^{\bullet-}$ quenching between $Ru^{II}b_2m^{\bullet-} \rightarrow$ ANQ electron transfer to give the RS state (reaction (*e*) in Scheme 2) and $Ru^{II}b_2m^{\bullet-} \rightarrow PTZ^{\bullet+}$ electron transfer to return to the ground state (reaction (*d*)).

Pathway for Back Electron Transfer. Referring to Scheme 2, there are three possible mechanisms for back electron transfer: (1) direct $ANQ^{\bullet-} \rightarrow PTZ^{\bullet+}$ electron transfer, pathway (*i*) in Scheme 2; (2) $Ru^{II} \rightarrow PTZ^{\bullet+}$ electron transfer to give $ANQ^{\bullet-}-Ru^{III}(b_2m)^{3+}-$PTZ followed by rapid $ANQ^{\bullet-} \rightarrow Ru^{III}$ electron transfer, pathway (*g*), and (3) $ANQ^{\bullet-} \rightarrow$ m electron transfer to give $ANQ-Ru^{II}(b_2m^{\bullet-})^{+}-PTZ^{\bullet+}$ followed by rapid $m^{\bullet-} \rightarrow PTZ^{\bullet+}$ electron transfer, pathway (*d*). For the two indirect mechanisms, the first step would necessarily be rate determining because $ANQ^{\bullet-}$ and $PTZ^{\bullet+}$ disappear simultaneously.

Mechanism (2) can be ruled out on the basis of the 0.6−0.7 eV energy content of the intermediate $ANQ^{\bullet-}-Ru^{III}(b_2m)^{3+}-$PTZ state. With a barrier of this magnitude, the maximum rate constant for back electron transfer would necessarily be several orders of magnitude lower than the experimental values. Similarly, but less directly, it is possible to rule out mechanism (3). From the data in Table 1, $\Delta G°$ for the initial step (which represents the minimum free energy of activation, $\Delta G^{‡}$) varies from 0.11 to 0.48 eV in the four solvents studied. This variation would result in a rate constant variation of $\sim 10^6$ if $\Delta G° = \Delta G^{‡}$. The actual variation is less than a factor of 2, Table 5.

Based on this analysis, back electron transfer occurs by mechanism (1) and direct $ANQ^{\bullet-} \rightarrow PTZ^{\bullet+}$ electron transfer. The free energy changes associated with back electron transfer, Table 5, were estimated from the differences in redox potentials between the $PTZ^{+/0}$ and $ANQ^{0/-}$ couples, $\Delta E_{1/2} = E_{1/2}(PTZ^{+/0}) - E_{1/2}(ANQ^{0/-})$, by using eq 7. The resulting $\Delta G°$ values reveal that back electron transfer is highly favored and occurs in the inverted region where $|\Delta G°| > \lambda$, where λ is the total reorganizational energy, solvent and intramolecular.

Back Electron Transfer in the Inverted Region. Back electron transfer is a nonradiative decay pathway for return of the redox-separated (RS) state to the ground state. Rate constants for $ANQ^{\bullet-} \rightarrow PTZ^{\bullet+}$ back electron transfer in all four solvents are listed in Table 5. As can be seen from the data, the rate constant for back electron transfer depends on the solvent.

From circular dichroism (CD) measurements in CH_3CN, and presumably in the other polar organic solvents as well, the preferred secondary structure of the oligoproline assembly is proline II.[13] As illustrated in Figure 2, in this structure the $PTZ^{\bullet+}-Ru^{II}-ANQ^{\bullet-}$ redox modules appear in a linear array aligned along the proline helix. In an orbital sense, $ANQ^{\bullet-} \rightarrow PTZ^{\bullet+}$ back electron transfer could occur through-bond through the seven intervening proline spacers and the 25 bonds that separate them. The extent of orbital mixing between the proline spacers and $PTZ^{\bullet+}$ should be greatly diminished due to the intervening $-CH_2CH_2-$ link.

Given recent results on the distance dependence of $Ru^{II}(b_2m^{\bullet-})^{+} \rightarrow PTZ^{\bullet+}$ electron transfer in a closely related series of proline assemblies, there may be an important and perhaps dominant role for through-space electron transfer.[45] For the proline II structure of **1**, an important component dictating the magnitude of $PTZ^{\bullet+}-ANQ^{\bullet-}$ electronic coupling could be charge-transfer super exchange through the intervening Rub_2m^{2+} chromophore.

In the inverted region, in the limits $-\Delta G° \gg S\hbar\omega$ and $\hbar\omega \gg k_BT$ and using the average mode approximation, k_{ET} is predicted to vary with $\Delta G°$ as shown in eqs 8 and 9.[26,31,48−50]

$$k_{ET} = \frac{2\pi}{\hbar}\frac{H_{DA}^{\ 2}}{(\hbar\omega(|\Delta G°| - \lambda_o))^{1/2}}\exp\left[-S - \frac{\gamma(|\Delta G°| - \lambda_o)}{\hbar\omega} + \left(\frac{\gamma+1}{\hbar\omega}\right)^2\lambda_o k_B T\right] \quad (8)$$

$$\gamma = \ln\left[\frac{|\Delta G°| - \lambda_o}{S\hbar\omega}\right] - 1 \quad (9)$$

H_{DA} is the electron-transfer matrix element, the resonance energy arising from orbital mixing between the $ANQ^{\bullet-}$ donor and $PTZ^{\bullet+}$ acceptor.

It is possible to estimate the magnitude of H_{DA} if the parameters in eq 8 can be independently evaluated. The solvent reorganization energies, λ_o, listed in Table 5 were calculated by using eq 10. Equation 10 is based on dielectric continuum theory and assumes nonpenetrating, spherical reactants. Equation 8 neglects the contribution from low-frequency vibrational modes treated classically.[31,39,51−54]

$$\lambda_o = e^2\left(\frac{1}{2a_1} + \frac{1}{2a_2} - \frac{1}{d}\right)\left(\frac{1}{D_{op}} - \frac{1}{D_s}\right) \quad (10)$$

In this equation, D_{op} and D_s are the optical and static dielectric constants of the medium and a_1 and a_2 are the radii of the ions. On the basis of the molecular modeling studies, we assume *d*, the through space center-to-center distance, to be 18 Å and the radii to be about 5 Å (Figure 2).

For $ANQ^{\bullet-} \rightarrow PTZ^{\bullet+}$ back electron transfer, the ring stretching modes from 1000 to 1600 cm^{-1} for both PTZ^{+}[34,55,56] and $ANQ^{\bullet-}$[34] are coupled to electron transfer and contribute to *S* and $\hbar\omega$ based on resonance Raman measurements. Quinone-based modes at 1340 and 1506 cm^{-1} also contribute.[34,56,57] In using eq 8 to calculate H_{DA}, we used $\hbar\omega = 1500$ cm^{-1} and $S = 2.5$. These values are consistent with values needed to account for the dependence of $\ln(k_{ET})$ on $\Delta G°$ in the work of Closs and Miller[31,58] ($\hbar\omega = 1500$ cm^{-1} and $S = 2.4$) and for $bpy^{\bullet-} \rightarrow PTZ^{\bullet+}$ electron transfer in $[Re(bpy^{\bullet-})(CO)_3(py\text{-}PTZ^{\bullet+})]^{+}$ (py-PTZ is 10-(4-picolyl)phenothiazine) ($\hbar\omega = 1450$ cm^{-1} and $S = 2.5$).[29,31]

Calculated H_{DA} values are listed in Table 5. Variations in *S* values of 2.5 ± 0.5 or in $\hbar\omega$ of 1500 ± 300 cm^{-1} cause variations in H_{DA} of ±15%. H_{DA} is small ($\sim$0.13 cm^{-1}) and in

(48) Bixon, M.; Jortner, J. *Faraday Discuss. Chem. Soc.* **1982**, *74*, 17.
(49) Brunschwig, B. S.; Sutin, N. *Comments Inorg. Chem.* **1987**, *6*, 209.
(50) Freed, K. F.; Jortner, J. *J. Chem. Phys.* **1970**, *52*, 6272.
(51) Barbara, P. F.; Meyer, T. J.; Ratner, M. A. *J. Phys. Chem.* **1996**, *100*, 13148.
(52) Hush, N. S. *Coord. Chem. Rev.* **1985**, *64*, 135.
(53) Marcus, R. A.; Sutin, N. *Biochim. Biophys. Acta* **1985**, *811*, 265.
(54) Marcus, R. A. *Rev. Mod. Phys.* **1993**, *65*, 599.
(55) Bodea, C.; Silberg, I. *Adv. Heterocycl. Chem.* **1968**, *9*, 321.
(56) Hester, R. E.; Williams, K. P. *J. Chem. Soc., Perkin Trans.* **1981**, *2*, 852.
(57) Vauthey, E.; Phillips, D.; Parker, A. W. *J. Phys. Chem.* **1992**, *96*, 7356.
(58) Closs, G. L.; Calcaterra, L. T.; Green, N. J.; Penfield, K. W.; Miller, J. R. *J. Phys. Chem.* **1986**, *90*, 3673.

the same range, H_{DA}= 0.08−0.22 cm^{-1}, as that found for electron transfer in $[(bpy)_2Ru^{III}L\text{-}(Pro)_n\text{-}apy\text{-}Ru^{II}\text{-}(NH_3)_5]^{5+}$ with n = 6, 7, 9 by Isied and co-workers.[59] Schanze and Cabana[60] calculated H_{DA} values of 10, 5, and 1 cm^{-1} for electron transfer in $Re^{I}(bpy^{\bullet-})(CO)_3\text{-}(Pro)_n\text{-}DMAB^{+}$ (DMAB is (dimethylamino)-benzoate) with n = 0, 1, and 2. For electron transfer in $[Re(bpy^{\bullet-})(CO)_3(py\text{-}PTZ^{\bullet+})]^{+}$, H_{DA} = 0.39 cm^{-1}.[29,31]

The results of Elliott, Steiner, and co-workers and Michel-Beyerle and co-workers show that interpretation of kinetically derived H_{DA} values for electron transfer that originate in excited-state quenching is potentially complicated by spin effects.[61,62] In $[Ru(bpy)_3]^{2+*}$, the initial MLCT "excited state" is actually a manifold of three Boltzmann-populated levels largely triplet in character arising from a lowest triplet state split by low symmetry and spin−orbit coupling.[63−65] For the electron-transfer quenching step, $Ru^{III}(b_2m^{\bullet-})^{2+*}-PTZ \rightarrow Ru^{II}(b_2m^{\bullet-})^{+}-PTZ^{\bullet+}$, the fraction of singlet products depends on the square of the singlet character of the initial excited state.[66] Because this is <10% for $[Ru(bpy)_3]^{2+*}$, the intermediate electron-transfer product is presumably nearly a pure triplet.

The triplet spin character is preserved in the second electron-transfer step to give the triplet RS state $^3(PTZ^{\bullet+}-ANQ^{\bullet-})$ as the dominant spin product.[62] Its return to the ground state, $^3(PTZ^{\bullet+}-ANQ^{\bullet-}) \rightarrow {}^1(PTZ-ANQ)$, is nominally spin forbidden. The spin restriction is lifted to the extent that spin−orbit coupling, largely through the heavy atom effect of the S atom in PTZ, mixes singlet character into the ^{3}RS intermediate.

There is an additional mechanism for return to the ground state (GS). It involves spin conversion in the RS state, $^3RS \rightarrow {}^1RS$, followed by $^1(PTZ^{\bullet+}-ANQ^{\bullet-}) \rightarrow {}^1(PTZ-ANQ)$ electron transfer.[62] There is no spin restriction for the final electron-transfer event in this case, and it is expected to be more rapid than $^3RS \rightarrow {}^1GS$ electron transfer by the square of the ratio of the singlet characters in ^{1}RS and ^{3}RS.[66]

The dominant mechanisms for $^3RS \rightarrow {}^1RS$ spin interconversion are anisotropic hyperfine coupling and electron spin−spin dipolar interactions. The ^{3}RS and ^{1}RS states are nearly degenerate because of the spatial separation of $PTZ^{\bullet+}$ and $ANQ^{\bullet-}$. In the absence of an external magnetic field, $^3RS \rightarrow {}^1RS$ interconversion is presumably rapid compared to back electron transfer.[62] In this dynamic limit, the value of $H_{DA} \approx 0.13$ cm^{-1} derived from the kinetic analysis is that arising from electronic coupling between $PTZ^{\bullet+}$ and $ANQ^{\bullet-}$,

$$H_{DA} = \langle(\pi^*_{ANQ})^1(\pi_{PTZ})^1|\hat{H}|(\pi^*_{ANQ})^0(\pi_{PTZ})^2\rangle\langle{}^1\psi_{s,i}|{}^1\psi_{s,f}\rangle$$

where π^*_{ANQ} and π_{PTZ} are the donor and acceptor orbitals. $\hat{H}$ is the operator mixing the wave functions, and $^1\psi_{s,i}$ and $^1\psi_{s,f}$ are the initial and final singlet spin wave functions with $\langle{}^1\psi_{s,i}|{}^1\psi_{s,f}\rangle = 1$.[66]

Conclusions

Quenching of the MLCT excited state of the Rubpy chromophore in **1** is dominated by $PTZ \rightarrow Ru^{II*}$ reductive electron transfer in the four solvents studied. Quenching occurs on the 10−20 ns time scale with solvent-dependent efficiencies that can exceed 0.9. Reductive quenching is followed by $Ru^{II}b_2m^{\bullet-} \rightarrow ANQ$ electron transfer to give the final redox-separated (RS) state, $PTZ^{\bullet+}-ANQ^{\bullet-}$, in competition with $Ru^{II}(b_2m^{\bullet-})^{+} \rightarrow PTZ^{\bullet+}$ electron transfer to return to the ground state. The formation efficiencies of the RS state are solvent dependent and vary from 33% (DCE) to 86% (ACN). Back electron transfer occurs in the inverted region and is also solvent dependent. The electron-transfer matrix element derived from an analysis of the kinetic data is $H_{DA} \approx 0.13$ cm^{-1}.

Synthesis of oligoproline redox triad **1** illustrates a general method for building assemblies having a spatially ordered array of functional sites protruding from a helical oligoproline framework. The modular approach adopted for the synthesis of **1** is quite general and can be extended readily to the construction of more complex assemblies. An attractive feature is that their properties can be predetermined by the nature of the functional groups added and by their relative spatial dispositions on the proline helix.

Acknowledgment. This work was supported by the National Science Foundation research grant CHE-9321413 (T.J.M.), and research grants from the John D. and Catherine T. MacArthur Foundation, grant SU-97-024 from the Camille and Henry Dreyfus Faculty Start-up Grant Program, and grant CC4634 from the Research Corporation Cottrell College Science Award (D.R.S.).

JA0304289

(59) Ogawa, M. Y.; Moreira, I.; Wishart, J. F.; Isied, S. S. *Chem. Phys.* **1993**, *176*, 589−600.
(60) Schanze, K. S.; Cabana, L. A. *J. Phys. Chem.* **1990**, *94*, 2740−2743.
(61) Gilch, P.; Pöllinger-Dammer, F.; Musewald, C.; Steiner, U. E.; Michel-Beyerle, M. E. *Science* **1998**, *281*, 982−984.
(62) Klumpp, T.; Linsenmann, M.; Bürssner, D.; Krissinel, E. B.; Larson, S. L.; Elliott, C. M.; Steiner, U. E. *J. Am. Chem. Soc.* **1999**, *121*, 1076−1087.
(63) Kober, E. M.; Meyer, T. J. *Inorg. Chem.* **1984**, *23*, 3877−3886.
(64) Hager, G. D.; Crosby, G. A. *J. Am. Chem. Soc.* **1975**, *97*, 7031−7037.
(65) Striplin, D. R.; Crosby, G. A. *Chem. Phys. Lett.* **1994**, *221*, 426−430.
(66) The electron-transfer matrix element for the quenching step, $H_{DA,q}$, is given by $H_{DA,q} = \langle(d\pi_3)^1(\pi_{PTZ})^2|\hat{H}|(d\pi_3)^2(\pi_{PTZ})^1\rangle\langle\psi_{s,i}|\psi_{s,f}\rangle$, with $d\pi_3$ and π_{PTZ} as the Ru- and PTZ-based acceptor and donor orbitals. H is the operator mixing the states, and $\psi_{s,i}$ and $\psi_{s,f}$ are the initial and final spin wave functions. The initial spin state can be written approximately as $\psi_{s,i} = {}^3\psi_i + \alpha{}^1\psi_i$, where $^3\psi_i$ is the pure triplet wave function, $^1\psi_i$ is the singlet wave function for a low-lying singlet, and α (which depends on the spin−orbit coupling constant and triplet−singlet energy gap) is the mixing coefficient. The rate constant for the quenching step depends on $H_{DA,q}^2$ (eq 8).